PERGAMON

International Journal of Solids and Structures 40 (2003) 4181–4190

INTERNATIONAL JOURNAL OF SOLIDS and STRUCTURES

www.elsevier.com/locate/ijsolstr

An experimental method for evaluating SIF distributions during crack turning in non-brittle materials

C.W. Smith *

Department of Engineering Science and Mechanics, Virginia Polytechnic Institute and State University, 219 Norris Hall, Blacksburg, Virginia 24061-0219, USA

Received 10 March 2003; received in revised form 10 March 2003

Abstract

After briefly describing an experimental modelling method consisting of a marriage of frozen stress photoelasticity with the Griffith–Irwin equations of fracture mechanics, the method is applied to a generic motor grain model containing part through cracks emanating from the corner of a fin tip under internal pressure to determine approximate crack shapes and stress intensity factor values at maximum crack depth for various penetration depths. The role of shear modes during crack turning is described.

Keywords: LEFM; Crack growth; Crack turning; Shear mode effects

1. Introduction

Since two well crafted papers by Cotterell (1965, 1966) describing crack types and paths in the mid 1960s, most of the literature concerning mixed mode effects on crack growth was directed towards the establishment of fracture criteria. Then in 1979, Cotterell and Rice (1980) provided an analysis which described the role of the shear mode in crack kinking, or turning. Then, Rubenstein (1991), guided by experiments, postulated an analysis for the turning of cracks in non-brittle materials. All of the analysis cited above was directed towards two dimensional problems, although Cotterell, in his earlier work, conjectured that his descriptions of crack growth might be extended to three dimensional problems. Recently, Leblond (1997) and Leblond et al. (1997) provided a three dimensional framework for use in analyzing such problems within linear elastic fracture mechanics (LEFM) constraints when the crack configuration is known.

Beginning in the late 1960s, the writer and his graduate students began to study a way to provide experimental code validation for the many numerical solutions to three dimensional fracture problems which were appearing in the literature. The vast majority of these solutions were based upon LEFM and crack growth was artificially prescribed in the solutions. Due to the substantial cost of full scale testing on such

* Tel.: +1-540-2316159; fax: +1-540-2314574.
E-mail addresses: chsmith4@vt.edu, lisas@vt.edu (C.W. Smith).

0020-7683/03/$ - see front matter © 2003 Elsevier Science Ltd. All rights reserved.
doi:10.1016/S0020-7683(03)00202-6

structures as aircraft, missiles, nuclear pressure vessels and ships, a laboratory based model analysis was focused on in order to provide a bridge between the numerical analyst and the full scale test of structure or their components with the idea of reducing the extent of the latter in code validation programs.

2. Methods of analysis

The aim of the development of such a "bridge" was to create a marriage between known experimental methods and LEFM, with technical refinements being introduced as needed. The experimental methods consist of the use of frozen stress photoelasticity and high density moiré interferometry, the former of which is focused upon here.

The frozen stress method was introduced by Opel (1936). It involved utilizing the fact that some photoelastic materials exhibited essentially diphase mechanical response to change in temperature. Stress freezing materials possess the special characteristic of possessing a temperature, T_c, called the critical temperature, which is in the neighborhood of the glass transition temperature of the material. In simplest concept, if one visualizes the material as Kelvin-like in its behavior (Fig. 1) it will be slightly viscoelastic at room temperature, but when heated above T_c, the viscous coefficient (μ) vanishes and the material becomes linearly elastic with an elastic modulus of about one six hundredth of it's room temperature value and the material becomes incompressible. Furthermore, the stress fringe sensitivity of the material above T_c increases to a value of some 20 times the value at room temperature. When a photoelastic model of such a material is heated above T_c, and then loaded to produce stress fringes, it is then cooled very slowly back to room temperature retaining the fringes produced above T_c. Then, upon unloading, fringe recovery will be small due to the relatively low fringe sensitivity at room temperature, and the fringes produced above T_c will be retained along with the deformations but no live stress results. Consequently the model may be sliced into thin slices and analyzed as in two dimensional photoelasticity, but with the three dimensional effect embedded in the fringes. Since the slices are thin, and the number of fringes will be proportional to the slice thickness, it is necessary to optically increase the number of fringes for accurate analysis. Two standard

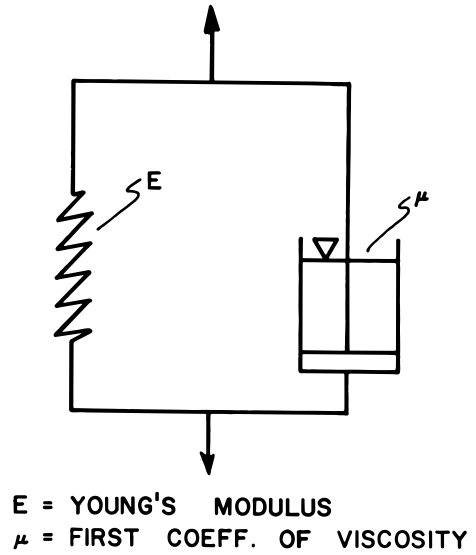

Fig. 1. Kelvin material.

methods, Post's (1966) Partial Mirror Fringe Multiplication and the Tardy (1929) Method are applied in tandem for this purpose.

Cracks are introduced into the model prior to heating. Artificial cracks are thin slots terminating at a point and natural cracks are made by striking a blade held against the surface of the model. A crack then emanates from the blade tip into the model and may be grown above T_c to desired size. The dimensions of the latter crack cannot be controlled but are believed to follow the path of fatigue cracks in metals growing stably. The load is then reduced to about a third of the value for growing the crack and stress freezing is carried out.

In order to convert the optical data embedded in the stress fringe patterns into the appropriate fracture parameter, the Stress Intensity Factor (SIF), one combines the stress-optic law with the Griffith–Irwin Equations for the near tip stress. This can be accomplished for all three local modes near the crack tip. The relevant algorithms are described in Smith and Kobayashi (1993) and also in Smith (1993), and are briefly described in Appendix A for Modes I and II.

3. Experiments

The applicability of the frozen stress approach to the determination of SIF distributions has been applied to a variety of problems Smith (2000). Recently, the Frozen Stress Method was used in order to study the crack growth and SIF distributions in cracks emanating from the fin tip surface of a generic rocket motor grain photoelastic model. Two dimensional experiments by AFRL at Edwards AFB suggested that cracks tend to initiate at the locus along the fin tip where the main tip radius coalesces with a much smaller corner radius. However, some manufacturers report cracks initiating on the axis of symmetry of a fin, possibly resulting from imperfections collected there due to the casting process.

The present study included tests on six models of geometry identical to Fig. 2, with two cracks, each analyzed independently in each model and with each cracked fin separated by an uncracked fin as shown. Two types of natural starter cracks were employed. One type was located on the fin axis in a plane of symmetry with respect to both the internal pressure loading and the model geometry. This type of crack, referred to as a "symmetric" crack, remained planar during growth and exhibited only pure Mode I values around the crack front. Moreover, it conformed to the definition of a Class I crack as described by Cotterell (1965). The second type of crack emanated from the point of confluence of the main fin tip radius (R11 in Fig. 2) with a much smaller edge radius (R1 · 3 of Fig. 2). This latter crack was non-planar and generally contained, prior to turning, mixed mode SIF values at various locations along its border except near the fin surface where Mode I prevailed. These cracks, due to turning, grew in arbitrary directions until turning eliminated the shear mode effects and so were essentially Class II cracks as described by Cotterell (1965) until the shear modes were eliminated, after which the cracks grew as Class I cracks exhibiting pure Mode I loading. These latter cracks are referred to here as "off-axis" cracks and the present discussion will focus on these cracks.

In the present study all off-axis cracks were analyzed for SIF values by using dimensions of planar projections of the crack fronts as their semi-elliptical dimensions since the out-of-plane dimensions of the crack surfaces were small (except for river markings), and eventually disappeared with the shear modes during growth. The study covered a range of a/c (depth to half length) values of 0.50–0.92 and a range of a/t (depth to thickness) values of 0.20–0.68.

Two principal types of off-axis cracks were observed and are pictured in Fig. 3. Model 4 depicts a slightly non-planar starter crack followed by more pronounced turning during growth along the crack front as indicated by the path of the centerpoint; said turning apparently due to Mode II. Moreover, at the crack front, both Mode I and Mode II SIF values were obtained along the crack border. Model 8i shows an additional effect. Radial river markings suggested the presence of a Mode III effect involving rather large

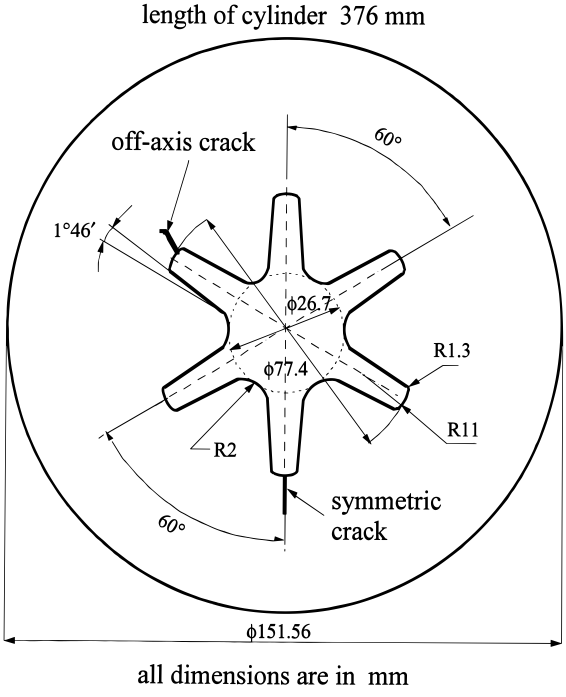

Fig. 2. Model dimensions and crack locations.

deformations of part of a crack surface normal to the adjacent surface (as well as Mode II) in the region between the fin surface and the final crack front. This effect appeared to be exacerbated by slight misalignment of the starter crack blade in the fin surface. Shear mode effects from crack tilting are depicted qualitatively in Fig. 4. At the stage of growth depicted in Fig. 3, no Mode II existed along the crack front. Data and results at maximum depth of the cracks for the above noted models and other off-axis crack models are presented in Table 1. Use of the algorithms for computing F_i is shown in Appendix A. Since the river markings appeared to involve large deformations, no SIF calculations were made for any of the modes in that region, confining such calculations primarily to maximum crack depth and near the fin surface.

4. Discussion

The symmetric cracks showed no shear mode or non-planar behavior, so results from these cracks are not included. However, it was quite apparent that these cracks grew far more readily than the off-axis cracks, and that the shear modes in the latter significantly slowed crack growth until the Class I condition was achieved in them. In fact, this effect is pictured in Model 8i as a dimple in the crack front (Fig. 3) due to the shear mode effect. In Model 4, the presence of Mode II retards the crack growth rather uniformly along the crack front except near the fin surface where Mode II is absent. One may conjecture that, if Model 8i were allowed to extend further once it has attained pure Mode I all along the crack border, the planar projection of the crack front would gradually approach a semi-ellipse.

Due to the complexities in the geometry of the off-axis cracks, a number of simplifying assumptions were made in achieving the determination of SIF values. To begin with, since none of the cracks deviated significantly from a semi-elliptic shape when projected onto a plane, and since the out of plane excursions were

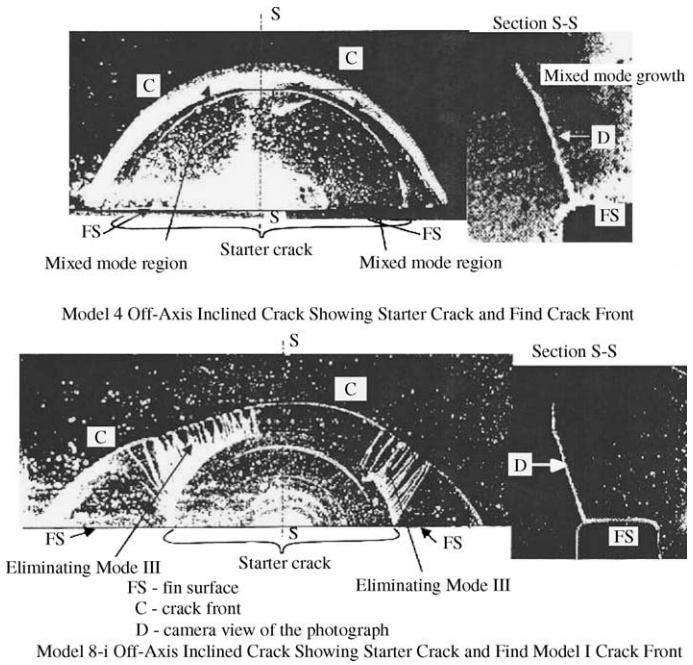

Fig. 3. Features of off-axis cracks initially normal to fin surface.

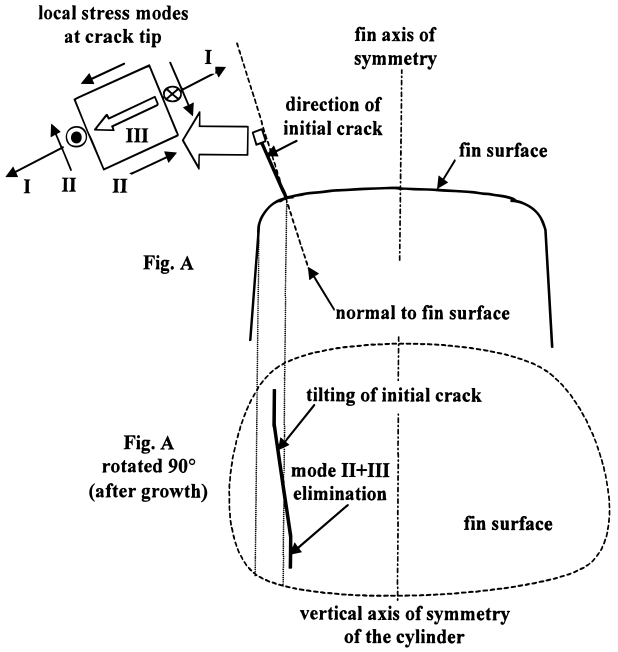

Fig. 4. Effect of misalignment and turning of starter crack blade.

Table 1
Data and results

Loads[a]	Crack description[b] (dimensions in mm)	F_1[c]
$P = 88.97$ N; $P_{max} = 0.049$ MPa; $P_{xf} = 0.035$ MPa	Model 4 Off-axis inclined $a = 8.71$; $\Delta a = 2.18$; $c = 11.15$; $\Delta c = 3.02$; $a/c = 0.78$; $a/t = 0.23$	$F_1 = 1.90$; $F_2 = 0.48$
$P = 88.97$ N; $P_{max} = 0.103$ MPa; $P_{xf} = 0.049$ MPa	Model 8i Off-axis inclined $a = 12.50$; $\Delta a = 3.4$; $c = 21.1$; $\Delta c = 10.4$; $a/c = 0.59$; $a/t = 0.34$	1.99
$P = 88.97$ N; $P_{max} = 0.049$ MPa; $P_{xf} = 0.035$ MPa	Model 6 Off-axis straight in $a = 11.60$; $\Delta a = 4.67$; $c = 17.00$; $\Delta c = 10.66$; $a/c = 0.68$; $a/t = 0.31$ Off-axis straight in $a = 11.23$; $\Delta a = 5.86$; $c = 13.00$; $\Delta c = 6.65$; $a/c = 0.86$; $a/t = 0.30$	1.72 1.86
$P = 88.97$ N; $P_{max} = 0.103$ MPa; $P_{xf} = 0.049$ MPa	Model 7 Off-axis straight in $a = 15.60$; $\Delta a = 10.0$; $c = 26.45$; $\Delta c = 17.57$; $a/c = 0.59$; $a/t = 0.42$ Off-axis straight in $a = 13.90$; $\Delta a = 4.05$; $c = 18.65$; $\Delta c = 10.17$; $a/c = 0.74$; $a/t = 0.37$	1.58 1.87
$P = 88.97$ N; $P_{max} = 0.103$ MPa; $P_{xf} = 0.049$ MPa	Model 8-s Off-axis straight in $a = 7.90$; $\Delta a = 2.8$; $c = 13.35$; $\Delta c = 7.75$; $a/c = 0.59$; $a/t = 0.21$	1.93
$P = 88.97$ N; $P_{max} = 0.103$ MPa; $P_{xf} = 0.049$ MPa	Model 9 Off-axis straight in $a = 25.10$; $\Delta a = 18.7$; $c = 39.4$; $\Delta c = 33.8$; $a/c = 0.64$; $a/t = 0.68$	1.50

[a] P = axial compressive load; P_{max} = internal pressure to grow crack; P_{xf} = stress freezing pressure.
[b] a = crack depth; Δa = crack growth; c = half length of crack in fin tip surface; Δc = half crack growth in fin tip surface.
[c] $F_1 = K_i\sqrt{Q}/P_{xf}\sqrt{\pi a}$, $i = 1, 2$ at maximum depth; $\sqrt{Q}$ = approximation of elliptic integral of second kind; $Q = 1 + 1.464(a/c)^{1.65}$, $a/c \leqslant 1$. All flaws were characterized as semi-elliptic flaws of depth a and length $2c$. However, off-axis cracks were neither perfect semi-elliptic nor planar.

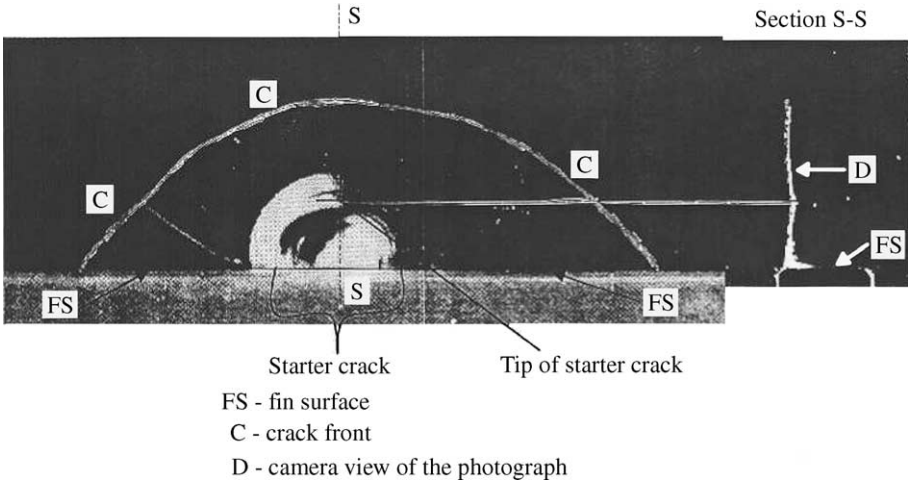

Fig. 5. Features of cracks when blade was parallel to fin axis.

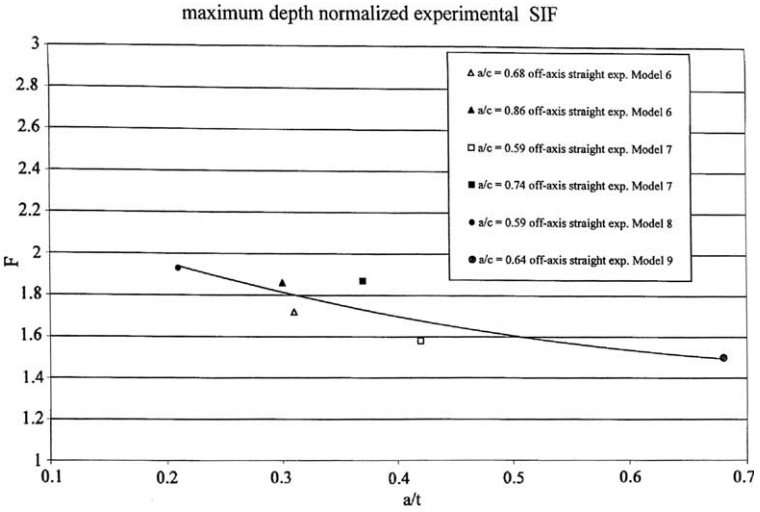

Fig. 6. Variation of normalized Mode I SIF with crack penetration depth.

small and virtually disappeared with crack growth after the shear modes were eliminated, they were treated as semi-elliptic cracks and appropriate approximations were used as defined in the bottom of Table 1. Secondly, when river markings occurred, they were taken as evidence of Mode III but suggested that LEFM limits were exceeded. No account was taken of the possible interaction between Mode III and the other modes in computing SIF values for the first two modes. Thirdly, very small misalignment of the crack blade across the fin surface at the critical off-axis location appeared to exacerbate the development of river markings as noted earlier. All of these assumptions may have been violated to some extent by the shorter cracks during their turning. However, once the cracks grew away from the fin surface and turning was completed, Class I behavior was restored and in this regime, results are likely not greatly affected by the above approximations.

The last six cracks listed in Table 1 were made by holding the striking blade parallel to the fin axis rather than normal to the fin surface. In these tests, slight damage occurred initially to the surface material but the portion of the crack length which indicated turning was minimized leading to an earlier development of the Class I crack along the crack front with only a couple of river marks (Fig. 5). By using only data from those tests where the blade was held parallel to the fin axis at the off-axis position, the resulting Mode I SIF at maximum depth showed a decreasing trend from $a/t = 0.2$ to $a/t = 0.68$ with data scatter of about 6%, the order of accuracy of the test (Fig. 6). Crack growth in these cases in the depth direction was 30–75% of the final crack length with the smaller growth cases deviating the most from the curve, and their crack shapes showing the greatest deviation from a projected semi-ellipse. All of these cracks grew first primarily in the fin surface until a certain length was reached after which they grew in the depth direction until the pressure was reduced for stress freezing. In a few cases, crack growth continued in the depth direction until the outer wall was penetrated without further growth in the fin surface. This suggests that growth in the fin surface is limited by, perhaps, the body geometry. In three cases (two symmetric and one off-axis straight) where the crack broke through to the outer surface, the value of a/c at break through was 0.8 ± 0.1.

5. Summary

An experimental study using the frozen stress method was conducted on generic photoelastic models of cracked motor grain. The study focused on the process of crack turning in a non-brittle material. Com-

plexities involved in the three dimensional turning effect including non-planar growth and river marking development produced Class II crack growth until the shear modes involved in the off-axis cracks were eliminated, resulting in Class I crack growth thereafter. Once Class I growth had been achieved, limited data showed a gradual decrease in the normalized Mode I SIF (F_1) with increasing crack depth from $a/t = 0.3$ to $a/t \approx 0.7$. Finally, when combined with results from symmetric cracks, it is clear that the latter cracks, originating as Class I cracks are far more serious than those emanating from the analytically predicted maximum stress at the off axis location.

Acknowledgements

The author wishes to acknowledge the support of the National Science Foundation for the development of the methods of analysis and ERC Inc. through the Air Force Research Laboratory for the tests described herein under RP010230. He also wishes to recognize the contributions of D.M. Constantinescu who conducted the tests and C.T. Liu for his ideas for the work. Finally, the author wishes to congratulate Professor Arthur Leissa on his many outstanding contributions to the field of Applied Mechanics.

Appendix A

Mode I Algorithm

Beginning with the Griffith–Irwin Equations, we may write, for Mode I, for the homogeneous case,

$$\sigma_{ij} = \frac{K_1}{(2\pi r)^{1/2}} f_{ij}(\theta) + \sigma_{ij}^0 \quad (i,j = n,z) \tag{A.1}$$

where σ_{ij} are components of stress, K_1 is SIF, r, θ are measured from crack tip (Fig. 7), σ_{ij}^0 are non-singular stress components.

Then, along $\theta = \pi/2$, after truncating σ_{ij}

$$\tau_{nz}^{\max} = \frac{K_1}{(8\pi r)^{1/2}} + r^0 = \frac{K_{\mathrm{AP}}}{(8\pi r)^{1/2}} \tag{A.2}$$

where $\tau^0 = f(\sigma_{ij}^0)$ and is constant over the data range, $K_{\mathrm{AP}} =$ apparent SIF, $\tau_{nz}^{\max} =$ maximum shear stress in nz plane.

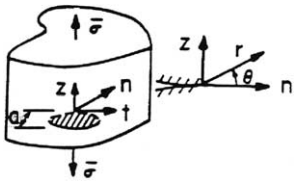

Fig. 7. Near tip notation for Mode I.

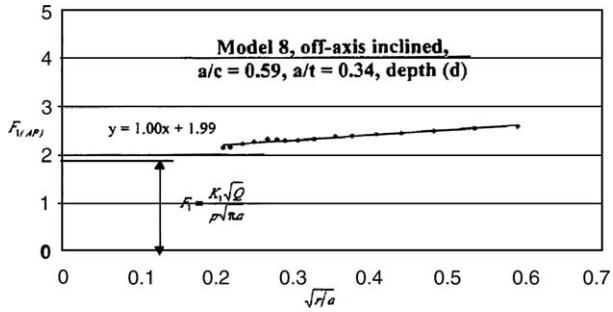

Fig. 8. Determination of F_1 from test data.

Normalizing with respect to $\bar{\sigma}$,

$$\therefore \frac{K_{AP}}{\bar{\sigma}(\pi a)^{1/2}} = \frac{K_1}{\bar{\sigma}(\pi a)^{1/2}} + \frac{\sqrt{8}\tau^0}{\bar{\sigma}}\left(\frac{r}{a}\right)^{1/2} \tag{A.3}$$

where (Fig. 7) $a =$ crack length, and $\bar{\sigma} =$ remote normal stress i.e $K_{AP}/(\bar{\sigma}(\pi a)^{1/2})$ vs. $\sqrt{r/a}$ is linear.

From the stress-optic law, $\tau_{nz}^{max} = nf/2t$ where, $n =$ stress fringe order, $f =$ material fringe value, and $t =$ specimen (or slice) thickness then from Eq. (A.2)

$$K_{AP} = \tau_{nz}^{max}(8\pi r)^{1/2} = \frac{nf}{2t}(8\pi r)^{1/2}$$

where K_{AP} (through a measure of n) and r become the measured quantities from the stress fringe pattern at different points in the pattern.

In the present study, instead of normalizing K with respect to $\bar{\sigma}(\pi a)^{1/2}$, we have selected $p\sqrt{\pi a/Q}$ as the normalizing factor where $\sqrt{Q}$ is an elliptic integral of the second kind approximated here, as shown in Table 1. An example of the determination of F_1 in Table 1 from test data is given in Fig. 8.

Mixed Mode Algorithm

The mixed mode algorithm was developed (see Fig. 9) by requiring that:

$$\lim_{\substack{r_m \to 0 \\ \Theta_m \to \Theta_m^0}} \left\{ (8\pi r_m)^{1/2} \frac{\delta(\tau)_{nz}^{max}}{\delta\Theta}(K_1, K_2, r_m, \Theta_m, \tau_{ij}) \right\} = 0 \tag{A.4}$$

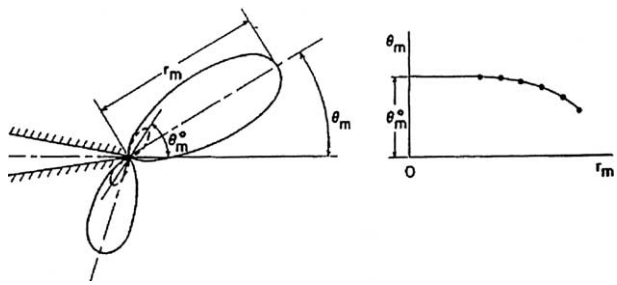

Fig. 9. Determination of θ_m^0 for mixed mode loading.

which leads to

$$\left(\frac{K_2}{K_1}\right)^2 - \frac{4}{3}\left(\frac{K_2}{K_1}\right)\cot 2\Theta_m^0 - \frac{1}{3} = 0 \tag{A.5}$$

By measuring Θ_m^0 which is approximately in the direction of the applied load, K_2/K_1 can be determined.

Then writing the stress-optic law as

$$\tau_{nz}^{\max} = \frac{fn}{2t} = \frac{K_{\mathrm{AP}}^*}{(8\pi r)^{1/2}}$$

where K_{AP}^* is the mixed mode of SIF, one may plot $K_{\mathrm{AP}}^*/(\bar{\sigma}(\pi a)^{1/2})$ vs. $\sqrt{r/a}$ as before, locate a linear zone and extrapolate to $r = 0$ to obtain K^*. Knowing, K^*, K_2/K_1 and Θ_m^0, values of K_1 and K_2 may be determined since

$$K^* = [(K_1 \sin\Theta_m^0 + 2K_2 \cos\Theta_m^0)^2 + (K_2 \sin\Theta_m^0)^2]^{1/2} \tag{A.6}$$

Knowing K^* and θ_m^0, K_1 and K_2 can be determined from Eqs. (A.5) and (A.6). Details are found in Smith and Kobayashi (1993).

References

Cotterell, B., 1965. On brittle fracture paths. International Journal of Fracture Mechanics 1, 96–103.

Cotterell, B., 1966. Notes on the paths and stability of cracks. International Journal of Fracture Mechanics 2, 526–533.

Cotterell, B., Rice, J.R., 1980. Slightly curved or kinked cracks. International Journal of Fracture 16 (2), 155–169.

Leblond, J.-B., 1997. Crack paths in three dimensional elastic solids I: two-term expansion of stress intensity factors—application to crack path stability in hydraulic fracturing. International Journal of Solids and Structures 36, 79–93.

Leblond, J.B., Lazarus, V., Mounchrif, S., 1997. Crack paths in three term expansion of the stress intensity factors—applications and perspectives. International Journal of Solids and Structures 36, 105–142.

Opel, G., 1936. Polarisationsoptische Untersuchung Räumlicher Spannungs-and-Dehnungszust ände. Forsch Geb Ingenieurw 7, 240–248.

Post, D., 1966. Fringe multiplication in three dimensional photoelasticity. Journal of Strain Analysis 1 (5), 380–388.

Rubenstein, A., 1991. Mechanics of crack path formation. International Journal of Fracture 47, 291–305.

Smith, C.W., 1993. Experimental determination of stress intensity factor distributions in engineering problems, Mechanics Pan America 1993. Applied Mechanics Reviews, Part 2 46 (11), 529–540.

Smith, C.W., 2000. An experimental method for measuring stress intensity factor distributions in three dimensional problems. Applied Mechanics Reviews 53 (4), R23–R32.

Smith, C.W., Kobayashi, A.S., 1993. Experimental fracture mechanics. Handbook on Experimental Mechanics, second revised ed. pp. 905–968 (Chapter 20).

Tardy, M.H.L., 1929. Methode Practique D'examen de Mesure de la Biréfringence des Verres D'optique Ref. Opt., vol. 8. pp. 59–69.